In-Phase, Anti-Phase and Fractured Synchrony in Ring Networks of Coupled Relaxation Electrochemical Oscillators

A. Karantonis,*,† M. Pagitsas,‡ Y. Miyakita,§ and S. Nakabayashi§

Department of Materials Science and Engineering, School of Chemical Engineering, National Technical University of Athens, Zografou 15780, Athens, Greece, Department of Chemistry, Faculty of Science, Aristotle University of Thessaloniki, Thessaloniki 54006, Greece, and Department of Chemistry, Faculty of Science, Saitama University, Saitama 338-8570, Japan

Received: January 16, 2004; In Final Form: February 18, 2004

The synchronization modes of coupled relaxation electrochemical oscillators are studied. The case of ring networks of discrete electrochemical oscillators is considered where boundaries are not present. A model of discrete coupled electrochemical oscillators is derived systematically from a continuous model and a discretization procedure. It is shown that, under specific conditions, the cells are coupled electrically and the connection is linear and symmetric. Also, the coupling strength is derived explicitly as a function of the geometric network characteristics, as well as the electric properties of the surrounding medium. The model equations are studied numerically, and the different modes of synchronization are discussed in detail. It is also shown that, because of fast transitions and the elimination of phase or period differences, networks of coupled relaxation electrochemical oscillators can perform some primitive information manipulation tasks.

1. Introduction

It is known, mainly from the field of mathematical biology, that the mechanism that leads to synchronized networks of nonlinear oscillatory cells is strongly dependent on the type of oscillator itself. Thus, nearly harmonic oscillators synchronize in a completely different manner and with a very different rate than relaxation oscillators.[1−3] Synchronization of coupled neurons is believed to be one of the possible ways of accomplishing sophisticated actions.[4,5] The uniqueness of the synchronization properties of networks of relaxation oscillators may be utilized in such a way that assemblies of coupled elements might perform some interesting information manipulation tasks.[6,7]

Despite the phenomenological resemblance between electrophysiological and electrochemical oscillators[8−13] and the large amount of work on electrochemical coupling and pattern formation,[14,15] there has not been any attempt to associate the observed synchronization modes of the latter with the waveform of the uncoupled oscillators. Only recently was it shown experimentally that networks of discrete coupled electrochemical oscillators of the relaxation type have unique synchronization features.[16,17]

In the present work, we address the question of whether, and under what conditions, an assembly of electrochemical cells can synchronize in various modes and how the synchronization features are affected by the waveform of the individual oscillators. For this reason, the synchronization modes of coupled electrochemical oscillators of relaxation type are studied. The case of ring networks of discrete electrochemical oscillators will be considered where boundaries are not present. To derive a model of coupled electrochemical oscillators systematically, we will start from a continuous ring electrode and follow a discretization procedure to describe the network. It will be shown that, under some specific conditions, the cells are coupled electrically and the coupling is linear and symmetric. Also, the coupling strength will be derived explicitly as a function of the geometric characteristics of the network, as well as the electric characteristics of the surrounding medium. After a brief description of a single relaxation oscillator, the equations will be studied numerically and the different modes of synchronization will be discussed in some detail. It will be shown also that, because of fast transitions and the elimination of phase or period differences, networks of coupled relaxation electrochemical oscillators can perform some primitive information manipulation tasks.

2. Rings of Discrete Oscillators

Let us consider a system that consists of a continuous working electrode located at $z = 0$ and a reference electrode located at a distance $z = w$ from the surface of the working electrode. The concentrations $c_m(x, y, z, t)$ and potential $\Phi(x, y, z, t)$ are governed by the Nerst-Planck equation,

$$\frac{\partial c_m}{\partial t} = D_m \nabla^2 c_m + n_m F \gamma_m \nabla(c_m \nabla \Phi) \tag{1}$$

with boundary conditions

$$j_{F,m} + j_{C,m} = -D_m \left.\frac{\partial c_m}{\partial z}\right|_{z=0} - n_m F \gamma_m c_m \left.\frac{\partial \Phi}{\partial z}\right|_{z=0} \tag{2}$$

$$c_m(x, y, z = w, t) = c_{b,m} \tag{3}$$

$$\Phi(x, y, z = w, t) = 0 \tag{4}$$

where $m = 1, ..., M$, and M is the number of ionic species. In the aforementioned equations, $j_{F,m}$ is the Faradaic flux due to the electrochemical reactions of the mth species and $j_{C,m}$ is the

* Author to whom correspondence should be addressed. E-mail: antkar@central.ntua.gr.
† National Technical University.
‡ Aristotle University.
§ Saitama University.

10.1021/jp049767u CCC: $27.50
Published on Web 04/13/2004

capacitance flux due to the transport of the mth species in charging the double layer. Apparently, the former is zero if the mth ionic species do not react electrochemically on the electrode. Analogously, the latter is zero if the mth species do not participate in charging the double layer. The diffusion coefficient D_m is assumed to be independent of concentration. The remaining symbols are the charge (n_m), the mobility (γ_m), and the Faraday constant (F). The concentration at the bulk of the solution ($c_{b,m}$) is assumed constant.

To derive a set of equations that describes an assembly of N discrete electrochemical oscillators forming a ring network, the following assumptions are introduced:

(1) The working electrode is considered to be a ring of radius l that consists of N discrete elements with a constant interdistance $2\pi l/N$.

(2) The reference electrode is an infinite plane, parallel to the plane that is defined by the ring network.

(3) The diffusion coefficients are equal: $D_1 = D_2 = ... = D$.

(4) The conductivity is approximately constant, even in regions of varying concentration.

(5) The spatial distribution of the ionic concentrations along the normal coordinate in a diffusion layer of length δ is considered linear.

(6) Only one electroactive species is present.

Under the aforementioned assumptions, a network of N discrete electrochemical oscillators in a ring geometry can be described by the following dimensionless equations (cf. Appendix A):

$$\epsilon\frac{du^{(k)}}{dt} = \frac{\sigma}{\beta}(\upsilon - u^{(k)}) - i_F(u^{(k)}, c^{(k)}) + \frac{\sigma\beta}{3h}\sum_{\substack{m=k-1\\ m\neq k}}^{k+1}(u^{(m)} - u^{(k)}) \tag{5}$$

$$\frac{dc^{(k)}}{dt} = 1 - c^{(k)} - \frac{t_c\sigma}{\beta}(\upsilon - u^{(k)}) + j_F(u^{(k)}, c^{(k)}) + \frac{\beta^2\xi^2}{2h}\sum_{\substack{m=k-1\\ m\neq k}}^{k+1}(c^{(m)} - c^{(k)}) - \frac{t_c\sigma\beta}{3h}\sum_{\substack{m=k-1\\ m\neq k}}^{k+1}(u^{(m)} - u^{(k)}) \tag{6}$$

for $k = 1, 2, ..., N$, and

$$[k] = k(\mathrm{mod}\ N) = \begin{bmatrix} N & (\text{for } k = 0)\\ k & (\text{for } k = 1, 2, ..., N)\\ 1 & (\text{for } k = N+1)\end{bmatrix} \tag{7}$$

In eqs 5 and 6, $u^{(k)}(t)$ and $c^{(k)}(t)$ are the double-layer potential and surface concentration of the kth oscillator, respectively. The functions i_F and j_F represent the total faradaic current and the faradaic flux of the electroactive species, respectively. The dimensionless parameters ϵ and σ represent the double-layer capacitance and the specific conductivity, respectively. The ratio of the distance between the reference electrode and the network and the length of the network is given by the parameter $\beta = 2\pi w/l$. For a constant interdistance $\Delta x = 2\pi/N$, the parameter h is defined as $h = \Delta x^2$. Finally, $\xi = \delta/w$ is the ratio of the length of the diffusion layer and the distance between the reference electrode and the ring network.

The coupling term in eq 5 is symmetric and linear. As discussed in previous studies,[18−20] it originates from a diffusion-like process that, upon discretization, represents next-neighbor coupling. For fixed h, σ, and l, coupling is enhanced as β increases, that is, as the reference electrode is brought away from the surface (increasing w) of the ring. In the absence of coupling, eq 5 corresponds to the usual ordinary differential equation (ODE) that describes only temporal variations of the double-layer potential, where the first right-hand term corresponds to the total current flowing through the cell and the second to the total faradaic current. The case of variable distance between the cells is treated in Appendix B.

In eq 6, two coupling terms exist: one that is due to concentration and another that is due to potential variations. Both terms are symmetric and linear. The coupling strength of the coupling due to mass transport is $\beta^2\xi^2/(2h)$. For fixed l, an increase of w will increase β but decrease ξ by the same amount, and, thus, the coupling strength remains fixed. Obviously, decreasing h increases the coupling strength.

For small ξ values ($\xi = \delta/w$), the coupling due to concentration variations can be ignored and eqs 5 and 6 can be written formally as

$$\epsilon\frac{du^{(k)}}{dt} = f_1(u^{(k)}, c^{(k)}) + \mu p_1{}^{(k)}(u^{(k-1)}, u^{(k)}, u^{(k+1)}) \tag{8}$$

$$\frac{dc^{(k)}}{dt} = f_2(u^{(k)}, c^{(k)}) + \mu p_2{}^{(k)}(u^{(k-1)}, u^{(k)}, u^{(k+1)}) \tag{9}$$

for $k = 1, ..., N$, $\mu = \beta\sigma/(3h)$ and $t_c = 1$. The coupling vector, $\boldsymbol{p}^{(k)} = (p_1{}^{(k)}, p_2{}^{(k)})$, will be

$$\boldsymbol{p}^{(k)} = \begin{pmatrix} u^{(k-1)} - 2u^{(k)} + u^{(k+1)}\\ -u^{(k-1)} + 2u^{(k)} - u^{(k+1)}\end{pmatrix} \tag{10}$$

For $\beta \ll 1$, it can be also assumed that the coupling term due to potential variations is considerably smaller than the rest of the right-hand terms of eq 6. Thus, the coupling vector is simplified even further:

$$\boldsymbol{p}^{(k)} = \begin{pmatrix} u^{(k-1)} - 2u^{(k)} + u^{(k+1)}\\ 0\end{pmatrix} \tag{11}$$

3. A Single Cell and Pairwise Coupling

For the total faradaic current, we assume a relationship of the form

$$i_F(u, c) = c(\alpha_1 u + \alpha_2 u^2 + \alpha_3 u^3) \tag{12}$$

Without loss of generality, for the faradaic flux, we assume a relationship of the form

$$j_F(u, c) = \alpha_0 i_F(u, c) \tag{13}$$

with $\alpha_0 < 1$. In addition, we consider the case where each element that belongs to the ring network is a relaxation oscillator ($\epsilon \ll 1$). For the coupling strength, we assume that it is weak (i.e., $\sigma\beta/(3h) \ll 1$) but finite. In some cases, we will insist also that $\sigma\beta/(3h) < \epsilon \ll 1$ The following is the optimal choice of the parameters: $\sigma/\beta = 0.1$, $\alpha_0 = 0.1$, $\alpha_1 = 1.125$, $\alpha_2 = -0.075$, and $\alpha_3 = 0.00125$.

By considering υ to be a bifurcation parameter of the system, we can plot the bifurcation curve, which corresponds to the steady-state polarization curve of a single electrochemical cell, $(\upsilon - u)$ vs υ. To do so, we utilize the AUTO program.[21] As can be seen in Figure 1a for small values of υ, the cell lies in a stable steady state that is denoted as *quiescent*. At $\upsilon = 26.800$, stable oscillations emerge, which disappear after a large increase of the period at $\upsilon \approx 29.243$. Furthermore, at $\upsilon = 29.590$ and $\upsilon = 29.235$, two saddle-node bifurcations occur. For $\upsilon > 29.246$, the system lies in another stable steady state, denoted as *silent*.

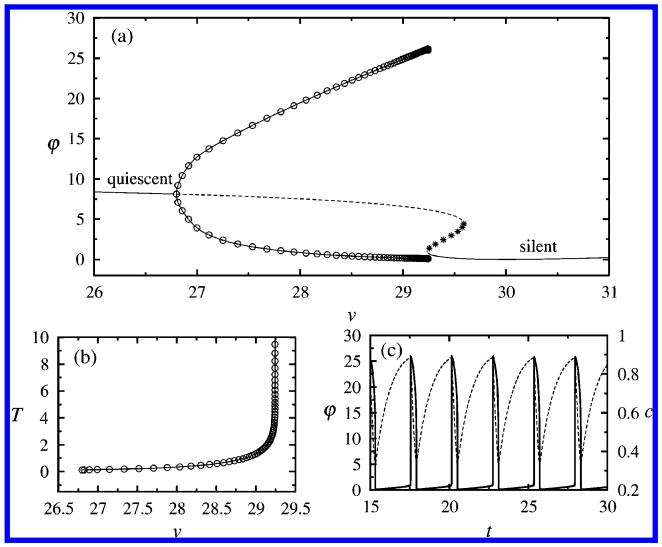

Figure 1. (a) Bifurcation curve for a single cell. Solid and dashed lines represent stable and unstable steady states, respectively ((*) saddle points and (○) minimum and maximum values of stable oscillations). (b) Effect of ν on the period T of a single oscillatory cell. (c) Temporal behavior of $\varphi(t) = \nu - u(t)$ and $c(t)$ for $\nu = 29.2$.

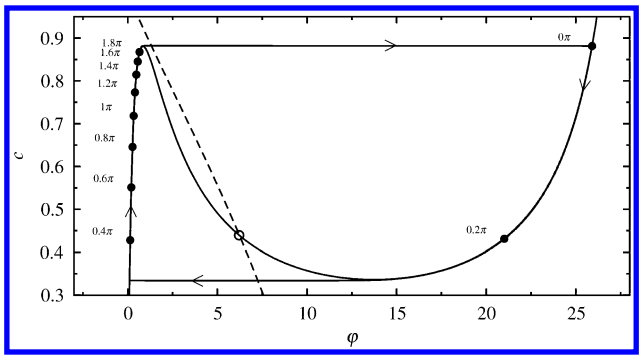

Figure 2. Nullclines of a single cell for $\nu = 29.2$, together with the relaxation limit cycle and the phase parametrization for $\epsilon = 1 \times 10^{-5}$: (—) $\dot{u} = 0$ nullcline and (— — —) $\dot{c} = 0$ nullcline).

The effect of ν on the period T can be seen in Figure 1b. In addition, Figure 1c shows an example of the temporal behavior of a single cell, for $\nu = 29.2$. From this figure, we must observe that, for sufficiently high ν values, the temporal evolution of $\varphi(t)$ (and, of course, $u(t)$) is of the relaxation type and also that the oscillator is predominately silent; that is, it spends considerably more time in the silent state than in the active state.

The nullclines of a single cell, together with the relaxation limit cycle for $\nu = 29.2$, are presented in Figure 2. The $f_1(u, c) = 0$ nullcline is an *N*-type curve, whereas the nullclines intersect at a single unstable point (noted by a white circle). The limit cycle for $\epsilon = 1 \times 10^{-5}$ lies on the two stable branches of the $f_1(u, c) = 0$ nullcline, with fast transitions between these two branches. Apparently, except in an ϵ neighborhood of the set

$$C = \{(u, c) | f_1(u, c) = 0\}$$

the vector field is almost horizontal:

$$\frac{dc}{du} = \frac{\epsilon f_2(u, c)}{f_1(u, c)} = O(\epsilon)$$

thus, the $f_1(u, c) = 0$ nullcline coincides with the *slow manifold* of the system. The time spend on the left (silent) branch is considerably longer than the time spend on the right (active) branch (see Figure 1c). Also, in Figure 2, the phase parametrization is presented. The point $\theta^{(k)}(0) = 0\pi$ is arbitrarily assigned to the peak of the oscillatory spike. The phase is assigned to each point of the limit cycle in a natural way by letting $\theta^{(k)}(t)$ be the solution to the phase equation

$$\dot{\theta}^{(k)} = \Omega^{(k)}$$

where $\Omega^{(k)} = 2\pi/T^{(k)}$ is the frequency of the uncoupled oscillator of period $T^{(k)}$.

Under weak coupling, each oscillator can be described by the phase equation[22−24]

$$\frac{d\phi^{(k)}}{dt} = \mu\omega^{(k)} + \mu H^{(k)}(\chi^{(k)}) \tag{14}$$

where $\phi^{(k)} = \Omega^{(k)}t - \theta^{(k)}$ is the phase deviation that accounts for the dynamical changes due to the weak connections and $\chi^{(k)}$ is the vector of phase differences with elements $\chi^{(i)} = \phi^{(i)} - \phi^{(k)}$ for $i = 1, 2, ..., N$. Also, $\omega^{(k)}$ accounts for small differences between the uncoupled oscillators. The T-periodic connecting function $H^{(k)}(\chi^{(k)})$ is given by

$$H^{(k)}(\chi^{(k)}) = \frac{1}{T}\int_0^T \boldsymbol{q}^{(k)}(t)\cdot\boldsymbol{p}^{(k)}(\Gamma(t, \chi))\, dt \tag{15}$$

where $\Gamma(t, \chi)$ is the vector of the uncoupled limit cycles with elements $\Gamma^{(i)}(t + \chi^{(i)})$. The vector $\boldsymbol{q}^{(k)}(t)$ is the solution of the equation adjoint to the linearized equation of the uncoupled system around the periodic solution

$$\frac{d\boldsymbol{q}^{(k)}}{dt} = -\boldsymbol{A}^{(k)}(\Gamma^{(k)}(t))^{\mathrm{T}}\boldsymbol{q}^{(k)}(t) \tag{16}$$

subjected to the normalization condition,

$$\frac{1}{T}\int_0^T \boldsymbol{q}^{(k)}(t)\cdot\boldsymbol{f}^{(k)}(t)\, dt = 1 \tag{17}$$

In eq 16, $\boldsymbol{A}^{(k)^{\mathrm{T}}}$ is the transpose of the Jacobian of the uncoupled system, calculated at the periodic orbit.[25]

In the case of next-neighbor diffusive coupling, the coupling term is written as

$$\boldsymbol{p}^{(k)} = \begin{pmatrix} u^{([k+1])}(\phi^{([k+1])} - \phi^{(k)} + t) - u^{(k)}(t) \\ 0 \end{pmatrix} + \begin{pmatrix} u^{([k-1])}(\phi^{([k-1])} - \phi^{(k)} + t) - u^{(k)}(t) \\ 0 \end{pmatrix} \tag{18}$$

Hence, the connecting function can be split into two terms:

$$H^{(k)}(\chi^{(k)}) = H_+^{(k)}(\phi^{([k+1])} - \phi^{(k)}) + H_-^{(k)}(\phi^{([k-1])} - \phi^{(k)}) \tag{19}$$

where $H_-^{(k)}$ and $H_+^{(k)}$ designate the connection to the previous and next neighbor, respectively. Similarly, the phase equation is written

$$\frac{d\phi^{(k)}}{d\tau} = \omega^{(k)} + H_+^{(k)}(\phi^{([k+1])} - \phi^{(k)}) + H_-^{(k)}(\phi^{([k-1])} - \phi^{(k)}) \tag{20}$$

where $\tau = \mu t$ is slow time. The equations that govern the evolution of phase differences can be formed by letting $\chi^{(k)} = \phi^{([k+1])} - \phi^{(k)}$. By considering identical oscillators ($\omega^{(1)} = ... = \omega^{(N)}$), the phase differences are governed by

$$\frac{d\chi^{(k)}}{d\tau} = H_+^{(k)}(\chi^{([k+1])}) + H_-^{(k)}(-\chi^{(k)}) - H_+^{(k)}(\chi^{(k)}) - H_-^{(k)}(-\chi^{([k-1])}) \quad (21)$$

Because the connections between the oscillators are diffusive and identical ($H_+ = H_-$), then $H_\pm(0) = 0$; thus, the in-phase synchronized solution always exists.

For the synchronized states of the degenerate case of only two oscillators, eqs 19 and 21 reduce to

$$\frac{d\chi}{d\tau} = H_-(-\chi) - H_+(\chi) = H(\chi) \quad (22)$$

where the phase difference $\chi = \phi^{(2)} - \phi^{(1)}$ is now a scalar. The steady states $\bar{\chi}$ will correspond to pairwise synchronized solutions of eqs 8 and 9. Furthermore, a synchronized solution will be stable if $\partial H(\bar{\chi})/\partial\chi < 0$.

In Figure 3a, we present the function $H(\chi)$ for the case in eq 11 and in Figure 3b for the case in eq 10, both for $\epsilon = 1 \times 10^{-5}$. In the first case, the system has three synchronized solutions, where the in-phase and anti-phase solutions are stable and the out-of-phase solution is unstable. In addition, we observe that $H(\chi)$ is almost discontinuous at the origin. This fact is expected for relaxation oscillators coupled through their fast variables and ensures that (a) the transition to in-phase synchronization is fast and (b) it persists under inhomogeneities of the frequencies of the individual oscillators.[23] On the other hand, although the anti-phase solution is stable, it is achieved after infinite time because $\chi(t)$ slows as this state is approached. The domain of attraction to the stable steady states is determined by the location of the unstable steady states. Thus, rapid in-phase synchronization is expected to be achieved for initial phase differences of $\chi \leq 0.273\pi$.

In the second case (Figure 3b), it can be seen that if there is also a connection between the fast and slow variables, there are only two solutions where the in-phase is stable and the anti-phase unstable; the discontinuity at the origin is also eliminated. Thus, in this case, we would expect only an in-phase solution, which is achieved after infinite time. The remainder of the paper involves only the case given in eq 11, which retains the unique properties of coupled relaxation oscillators. The coupling will be only in the fast ODE that describes the temporal evolution of the potential $u^{(k)}(t)$. The coupling strength is given by the term $\sigma\beta/(3h)$. In some cases, the results will be given in a three-dimensional representation but more often in a black-and-white binary representation. In the latter case, we set a threshold value (e.g., $\varphi = 10$) and we designate the system as active if the potential is above this threshold value. The active state of a cell is represented by black in the binary representation. All further calculations were performed by implementing an adaptive-step Runge−Kutta method (Fehlberg fifth-order with Cash and Karp constants).[26]

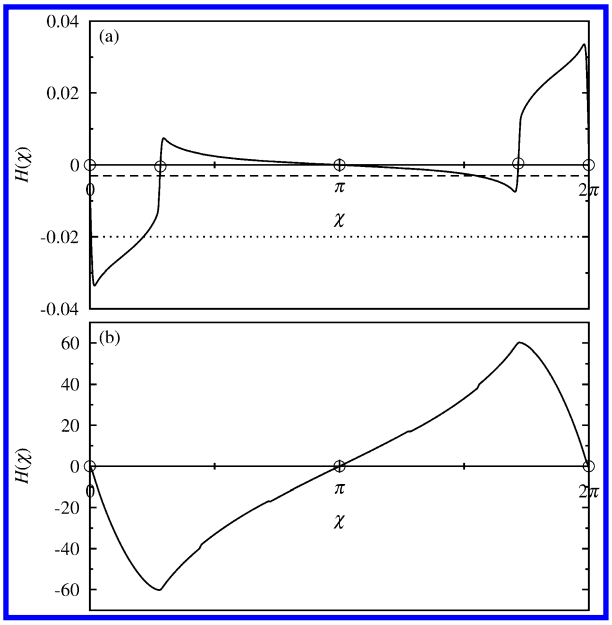

Figure 3. Connecting function for (a) coupling of the form given in eq 11 and (b) coupling of the form given in eq 10. In both cases, $\epsilon = 1 \times 10^{-5}$. Circles designate steady states; see text for the meaning of the dashed and dotted lines.

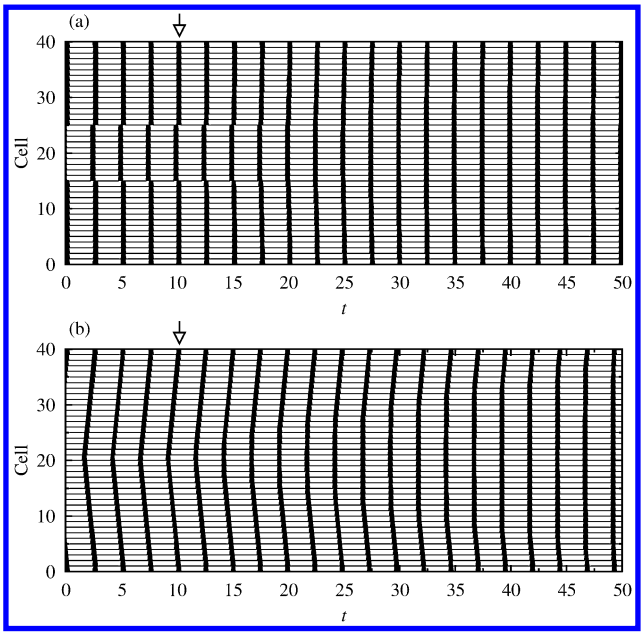

Figure 4. (a) In-phase synchronization of two groups starting with initial phase differences of 0.2π on the uncoupled limit cycle. (b) In-phase synchronization of a set with a linear gradient distribution of 0.8π of the initial phases on the uncoupled limit cycle. Coupling is made effective at the arrowed position. In both cases, $\sigma\beta/(3h) = 1 \times 10^{-5}$, $\epsilon = 1 \times 10^{-5}$, and $\upsilon = 29.2$.

4. In-Phase Synchronization by Phase Compensation

A main characteristic of relaxation oscillators that distinguishes them from oscillators of more harmonic character is that they synchronize in-phase relatively faster. In this section, it is shown that this situation is indeed valid in the present case, where communication is due to linear and symmetric electric coupling.

We will study a network of identical relaxation oscillators, the initial conditions on the *uncoupled* limit cycle, and relatively weak coupling. The initial conditions of a specific number of neighboring cells are set with a phase difference related to the remainder of the cells. In the specific example of Figure 4a, cells {16−25} initially have a phase difference of $\chi = 0.2\pi$ with the remaining cells. This choice of χ ensures that the system lies in the domain of attraction to the stable in-phase solution (Figure 3a). As shown (in the absence of coupling), the network initially consists of two groups oscillating with a phase difference χ. At $t = 10$, the coupling is made effective; as a result, the phase differences are rapidly eliminated and the network is synchronized in-phase. We refer to this phenomenon as in-phase synchronization due to phase compensation. Rapid phase compensation is observed for any initial phase differences χ that lie in the domain of attraction of the in-phase solution,

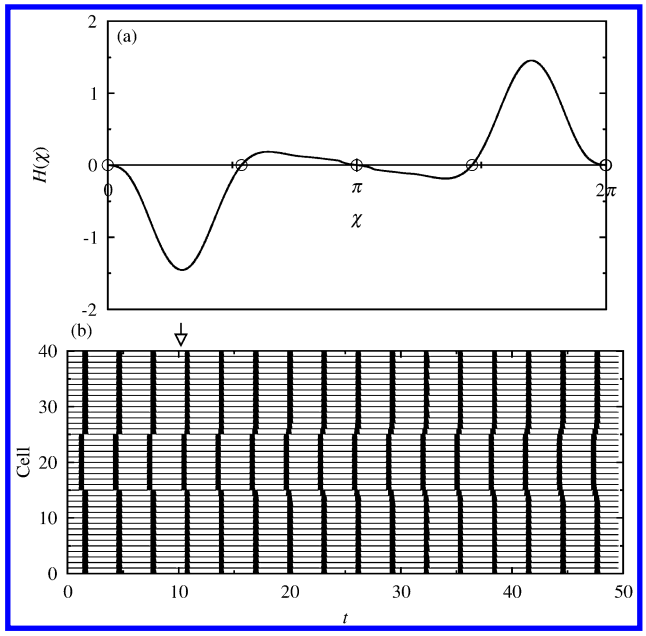

Figure 5. (a) Connecting function for oscillators with less relaxation character. Circles designate steady states. (b) Coupling of two groups starting with initial phase differences of 0.2π on the uncoupled limit cycle. Coupling is made effective at the arrowed position. For both figures, $\sigma\beta/(3h) = 1 \times 10^{-5}$, $\epsilon = 1 \times 10^{-3}$, and $\upsilon = 29.2$.

even if they are randomly distributed around the zero phase difference.

Other initial distributions also lead to phase compensation that results in an in-phase synchronization, as in the case of Figure 4b. In this specific example, we impose a linear gradient distribution 0.8π of the phases by imposing a linear increase of the phases starting from cell 20 and expanding in both directions. Initially, the coupling strength is set to a zero value and apparently cells preserve the imposed phase difference. At $t = 10$, coupling is enabled; as a result, the network rapidly synchronizes in-phase and phase differences are eliminated. Interestingly, $\chi = 0.8\pi$ lies outside of the domain of the attraction to the in-phase solution; however, because cells are capable of pairwise synchronization, the resulting behavior is stable in-phase synchrony.

For the sake of comparison, it is interesting to observe how oscillators with less relaxation character approach the in-phase synchronized solution. As shown in Figure 5a, when $\epsilon = 1 \times 10^{-3}$, three steady states exist for the connecting function $H(\chi)$. The in-phase and anti-phase solutions are stable, whereas the out-of-phase solution is unstable. Moreover, the domain of attraction to the in-phase synchronized solution is enlarged. Nevertheless, by comparing Figures 3a and 5a, it can be observed that the discontinuity at the origin has disappeared. As χ approaches zero, it is simultaneously slowed and, thus, in-phase synchrony would get considerably more time. This is indeed the situation, as can be observed in the example presented in Figure 5b. As observed previously, the two groups of oscillators are set with an initial phase difference of $\chi = 0.2\pi$. At $t = 10$, the coupling is made effective but in-phase synchronization is achieved slowly.

5. In-Phase Synchronization by Period Compensation

An additional feature of the in-phase synchronized state of coupled relaxation oscillators is that small period differences are eliminated. This property also is based on the discontinuity at $\chi = 0$ (Figure 3a), which exists at the relaxation limit.[23] Thus,

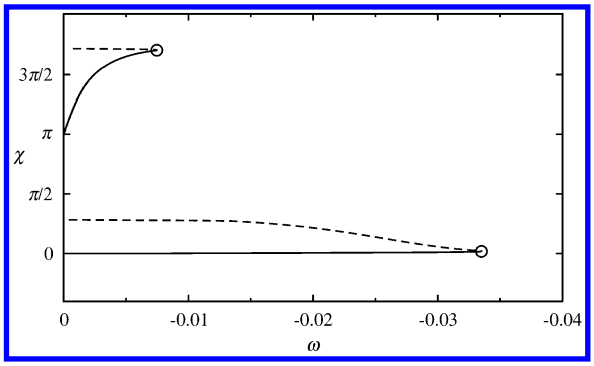

Figure 6. Partial bifurcation diagram of eq 23 for $\epsilon = 1 \times 10^{-5}$: (○) saddle-node bifurcations, (—) stable steady states, and (– – –) unstable steady states).

in the case of two slightly different oscillators and in the presence of small deviations ($\mu\Delta\omega_i$) from the common frequency, eq 22 is written as

$$\frac{d\chi}{d\tau} = \Delta\omega + H(\chi) \tag{23}$$

where $\Delta\omega = \omega_2 - \omega_1$. In this case, each root of the equation $\Delta\omega + H(\bar{\chi}) = 0$ corresponds to a synchronized solution with a phase difference $\bar{\chi}$. Graphically, this means that, in the presence of small period differences, the steady states are given by the points of intersection of the graph of $H(\chi)$ with the line $-\Delta\omega$. Hence, in the relaxation limit, the $\bar{\chi} = 0$ steady state persists, even in the presence of small $\Delta\omega$. Furthermore, the range of $\Delta\omega$ for which the in-phase synchronized solution exists is determined by the extrema values of the $H(\chi)$ function (see Figure 3a). On the other hand, by inspecting Figure 3a, it is straightforward to observe that the anti-phase solution does not persist under small period differences. Thus, for very small $\Delta\omega$, an out-of-phase stable solution co-exists with the in-phase solution (dashed line), whereas for slightly higher values of $\Delta\omega$, the in-phase solution is the only stable state (dotted line).

The influence of $\Delta\omega$ on the phase difference χ can be studied more easily if we plot the bifurcation diagram of eq 23 by considering $\Delta\omega$ as a bifurcation parameter. Figure 6shows that, for small absolute values of $\Delta\omega$, four steady states exist, two of them being stable. At $\Delta\omega \approx -0.00745$, the two upper steady states disappear via saddle-node bifurcation. For $\Delta\omega > -0.00745$, only two steady states exist, where $\bar{\chi} = 0$ is stable. Furthermore, these two steady states disappear after another saddle-node bifurcation at $\Delta\omega \approx -0.0335$. Obviously, the stable steady state $\bar{\chi} = 0$ exists over the entire interval $0 \leq \Delta\omega \leq -0.0335$.

6. Anti-Phase and Fractured Synchrony

After all cells in a ring network start to oscillate from almost in-phase initial conditions, they will rapidly synchronize by compensating the phase differences. Nevertheless, the anti-phase synchronized solution is also stable for ring networks of relaxation oscillators connected by electrical linear symmetric coupling (Figure 3a), because $\partial H(\pi)/\partial\chi < 0$. Although the anti-phase solution is stable, it does not have the same features, in regard to the in-phase synchronization. As shown in Figure 3a, a discontinuity is not present at $\chi = \pi$ and, as a result, the transition to anti-phase synchrony requires considerably longer time than the transition to in-phase locking.

The stability of the anti-phase solution can be observed in Figure 7a. In this figure, cells {16−24} start with initial conditions that are exactly anti-phase to the rest of the cells.

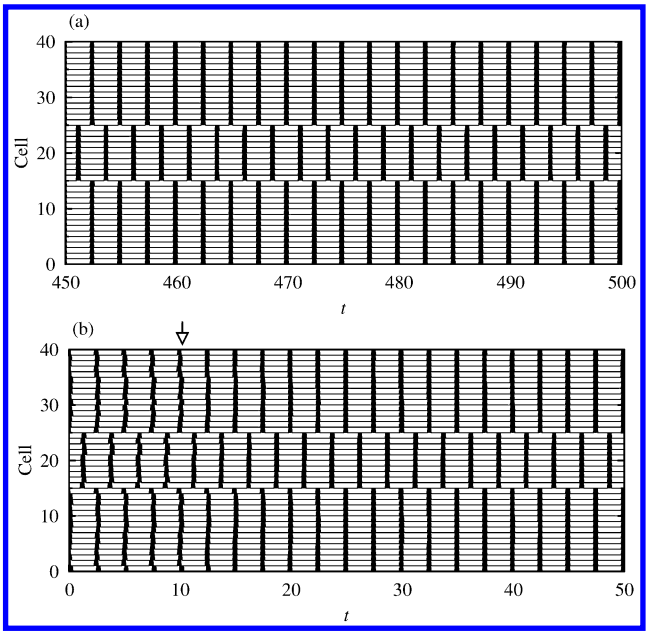

Figure 7. (a) Anti-phase synchronization of two groups starting at exact anti-phase, $\sigma\beta/(3h) = 1 \times 10^{-5}$. (b) Fractured synchrony of two groups, $\sigma\beta/(3h) = 1 \times 10^{-5}$. Arrowed feature indicates the initiation of coupling. For both figures, $\epsilon = 1 \times 10^{-5}$ and $\upsilon = 29.2$.

After a group of cells starts to oscillate exactly anti-phase with the rest of the oscillators, they remain anti-phase.

In the example of Figure 7b, the initial conditions of the central group are arranged on the uncoupled limit cycle with a random distribution (by means of Fortran's RAN function) around $\chi = \pi$. The same holds for the remaining cells, but the distribution is around $\chi = 0$. Initially, the cells are oscillating in the absence of coupling and, thus, the imposed phase differences are conserved. At $t = 10$, coupling is made effective; cells that belong to the same group rapidly synchronize in-phase, whereas the two groups are slowly synchronized into an anti-phase state. This phenomenon is also called as *fractured synchrony*.[3] Fractured synchrony can be explained qualitatively by considering the action of two boundary cells, oscillating anti-phase. Because the anti-phase solution is stable, these two cells will remain anti-phase and act as pacemakers for the remaining cells of the corresponding groups. The remaining cells of each group rapidly synchronize in-phase with the pacemaker and, as a result, the two groups synchronize anti-phase.

The ability of boundary cells to act as pacemakers, when the system is of a relaxation type, can be utilized to "imprint" the spatial pattern of the network through the initial conditions. Let us assume that our desire is to design a network where a specific combination of synchronized groups must exist. It is sufficient to impose exactly this desired pattern into the initial conditions by arranging the phase of each cell, without the necessity to alter the architecture of the network or the nature of connections. In addition, because relaxation oscillators compensate for small phase differences, an ambiguity in this initial information is allowed; coupled relaxation cells will rapidly eliminate the phase differences and synchronize according to the desired pattern.

The same generally is not true for oscillators with more harmonic character. In this case, a wavelike propagation is expected to occur but also the coupled response is expected to be dependent on the number of cells in each group.[3] In any case, the final state of the system is approached *very* slowly, in contrast to relaxation oscillators. In Figure 8a, the connecting function $H(\chi)$ is presented for $\epsilon = 2.5 \times 10^{-2}$. Obviously, the anti-phase solution is unstable and the stable in-phase solution

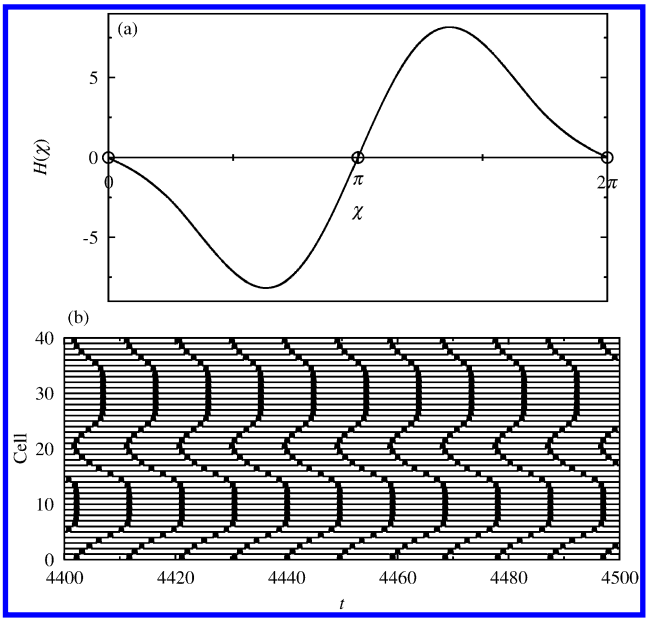

Figure 8. (a) Connecting function for oscillators with more harmonic character; circles designate steady states. (b) Coupling of two groups starting with anti-phase initial phase differences on the uncoupled limit cycle. For both figures, $\sigma\beta/(3h) = 1 \times 10^{-5}$, $\epsilon = 2.5 \times 10^{-2}$, and $\upsilon = 29.2$.

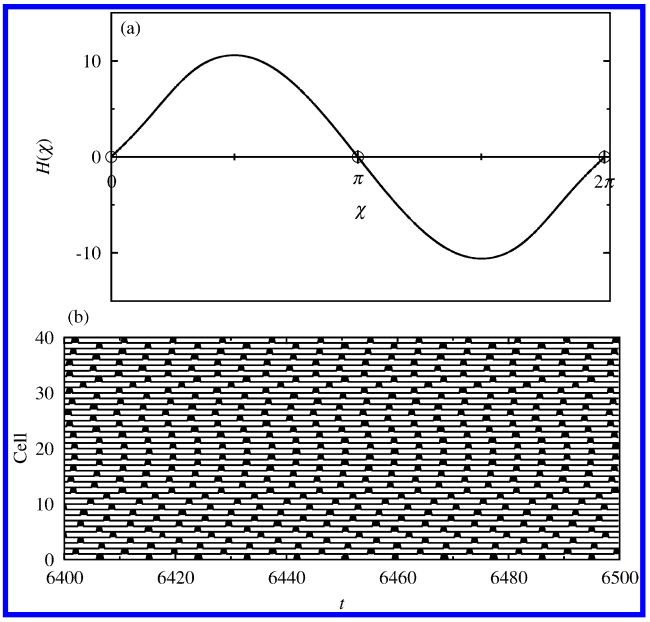

Figure 9. (a) Connecting function for oscillators of almost harmonic character; circles designate steady states. (b) Coupling of two groups starting with anti-phase initial phase differences on the uncoupled limit cycle. For both figures, $\sigma\beta/(3h) = 1 \times 10^{-5}$, $\epsilon = 5 \times 10^{-2}$, and $\upsilon = 29.2$.

is approached very slowly. The response of a network of 40 nonrelaxation oscillators, initially divided into two anti-phase groups, is presented in Figure 8b for $\epsilon = 2.5 \times 10^{-2}$. As can be observed, ever after a very long time, the in-phase behavior is not achieved.

The situation can be altered even more, if the individual oscillators are almost harmonic. As shown in Figure 9a for $\epsilon = 5 \times 10^{-2}$, the in-phase solution is unstable whereas the anti-phase solution is stable. In Figure 9b, initially, the network is divided into two groups with anti-phase initial conditions. The cells have an apparent tendency to synchronize in an "one-by-one" anti-phase manner; however, fractured synchrony is not observed. This is to be expected because the in-phase solution

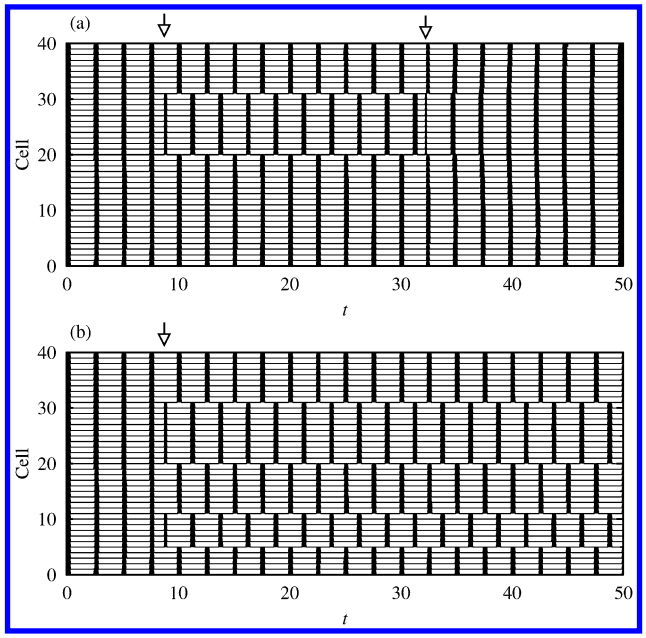

Figure 10. (a) Anti-phase synchronization induced by a single perturbation on cells {20−30}. (b) Single perturbation on cells {5−10} and {20−30}. Vertical arrows indicate the instant of perturbation. For both figures, $\epsilon = 1 \times 10^{-5}$ and $\sigma\beta/(3h) = 1 \times 10^{-5}$. See text for the characteristics of the pulse.

is unstable and, thus, cells have a tendency to approach a pairwise anti-phase state, which is stable.

7. Perturbation-Induced Anti-Phase Synchronization

In Section 6, we showed that information can be stored into the network by imprinting the phase differences in the initial conditions. In this section, we will show that information can be stored or removed from the network during the course of oscillations by perturbing the system locally.

If the coupling strength is weak and all cells in the network start from a slightly out-of-phase initial condition, all cells will rapidly synchronize in a common phase, i.e., the network will be synchronized in-phase. This phenomenon is what was called a compensation of phases in Section 4. Experimental evidence shows that this is the most probable state observed when almost identical electrochemical relaxation oscillators are coupled electrically.[16] In addition, we learned from Section 6 that if a group of cells starts from an anti-phase state, in relation to the remaining cells, then the groups will preserve a phase difference.

The aforementioned observations can help us to design a method of altering the in-phase synchronized state. Let us assume that, at a specific time instant and while the common synchronized state is almost at phase π, a group of cells is perturbed by a single perturbation. Let us choose phase π to be that observed while on the silent state of the oscillatory cycle. Thus, the effect of the perturbation is to force the members of this group to the active state, i.e. this group is forced to produce a single spike. After the spike is produced, the phase difference between this group and the rest of the network is π. Thus, the two groups will remain anti-phase, because this state is also stable.

An example of this procedure is presented in Figure 10a. Initially, all 40 coupled cells oscillate in complete in-phase synchrony. At $t = 8.75$, a potential pulse is applied with a duration of $\Delta t = 0.1$ and amplitude of $u_p = -0.1$ onto cells {20−30}. Observe that, at this instant, the network is indeed in its silent state and the phase is almost π. As expected, under the influence of this single pulse, cells {20−30} fire a spike. From that time forward, the phase difference between the cells {20−30} and the remainder is anti-phase. Thus, the "information" written to the network remains.

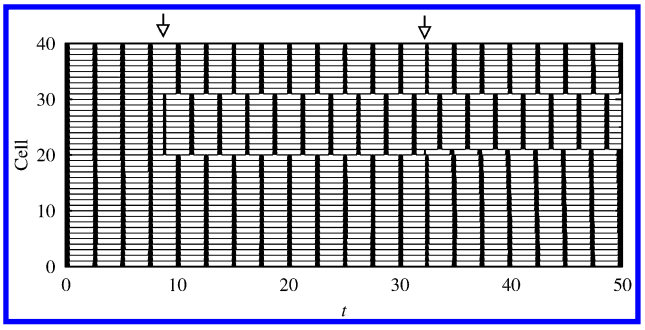

Figure 11. "Correction" of the induced pattern at $t = 32.25$. Cell 20 is forced into its neighboring group. Vertical arrows indicate the instants of perturbation. In this figure, $\epsilon = 1 \times 10^{-5}$ and $\sigma\beta/(3h) = 1 \times 10^{-5}$. See text for the characteristics of the pulse.

Interestingly, the "information" also can be removed from the network. This can be done by perturbing the same group at any phase instant with χ within the domain of the attraction to the in-phase solution. As shown in Figure 10a, when a single potential pulse is applied at $t = 32.25$, the group is rapidly synchronized with the remainder of the network and all previous information is erased.

It is possible to force more than one group into the anti-phase state within a specific network and thus produce a more complex pattern. For example, in Figure 10b, not only cells {20−30} but also cells {5−10} are perturbed at $t = 8.75$. As a result, the pattern consists of three different groups with a variable number of members oscillating in-phase or out-of-phase.

To some degree, the imputed information can be also corrected without a prior removal. The process can be easily deduced by the example presented in Figure 10a. Let us assume that cells {20−30} have been forced into an anti-phase state, but we later decide that cell 20 should belong to the other group instead. To "correct" the pattern, it is sufficient to perturb only cell 20 while its phase is in the domain of attraction of the in-phase state. Once this is accomplished, the cell will abandon its group and jump rapidly to the other group. An example is shown in Figure 11 where initially all 40 cells form a single in-phase synchronized group. At $t = 8.75$ we perturb cells {20−30} to the anti-phase state. At $t = 32.25$, it is decided that cell 20 would rather belong to the other group; a single pulse at this instant is adequate to perform the task.

8. Periodic Spiking due to Coupling

Up to this point, we have considered the case of coupled oscillatory cells. Nevertheless, it can be shown that a network of *nonoscillatory* cells can become oscillatory, because of linear symmetric electric coupling.

Once again, we consider a ring that consists of 40 cells, all being of the relaxation type ($\epsilon = 1 \times 10^{-5}$). Ten neighboring cells are lying in their stable silent steady state, close to the homoclinic bifurcation point ($\upsilon = 29.3$). The remaining cells are lying in the stable quiescent steady state, close to the Hopf bifurcation point, $\upsilon = 26.5$. Obviously, if coupling is not effective, all cells will remain in their corresponding steady states and oscillations are not observed. This is the case for $t < 5$ in Figure 12a. At a specific instant, $t = 5$, the coupling is turned on. The group of relaxation oscillators starts to fire while the remaining cells stay in the quiescent steady state. Interest-

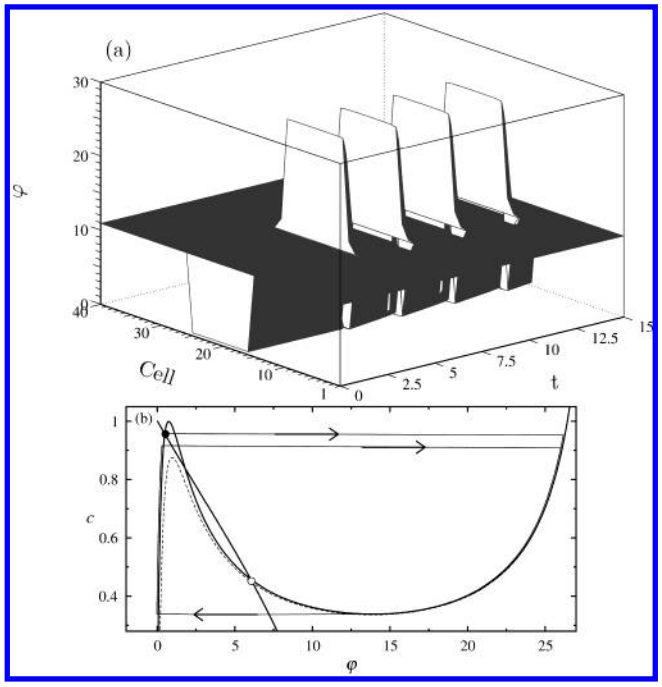

Figure 12. (a) Coupling of two non-oscillatory groups. Group {16−25} consists of relaxation oscillators lying on its stable silent steady state, $\upsilon = 29.3$. Cells {1−15} and {26−40} rest on the quiescent steady state, $\upsilon = 26.5$. The coupling strength is $\sigma\beta/(3h) = 1 \times 10^{-3}$. (b) Nullclines of a single relaxation oscillator lying on the silent steady state (full lines). Solid circle designates the stable steady state. At the instant of coupling, the $\dot{u} = 0$ nullcline is shifted downward (dashed line) and oscillations appear.

ingly, even though only boundary cells of the silent group are coupled with the quiescent cells, all members of the relaxation group also will fire and rapidly synchronize to a common phase, because of the relaxation character of the oscillators.[17] Note that similar synchronization of a silent group also is observed if the other group is oscillatory (either harmonic or relaxation) instead of quiescent.

The periodic spiking induced by coupling is easy to understand if we inspect the effect of the connections to the nullclines. If a cell k lies in the silent steady state, then the nullclines, $f_1^{(k)}(u, c) = 0$, $f_2^{(k)}(u, c) = 0$ are the ones shown by full lines in Figure 12b. There is only one stable steady state, denoted by a black circle. If the coupling strength is different than zero and if both neighbors—$(k - 1)$ and $(k + 1)$—of this cell are silent, then coupling has no effect. On the other hand, if one of the neighbors $(k - 1)$ is quiescent, then coupling is effective and it has the form $[\sigma\beta/(3h)](u^{(k-1)} - u^{(k)}) \approx [\sigma\beta/(3h)](u^{(k-1)} - \upsilon)$. Thus, because of the presence of the quiescent neighbor $k - 1$, a constant coupling is applied to cell k and the nullcline $f_1(u, c) = 0$ shifts to the new nullcline $f_1(u, c) + [\sigma\beta/(3h)](u^{(k-1)} - \upsilon) = 0$, as shown by the dashed line in Figure 12b. However, now, the silent state is no longer a steady state of the cell, and, hence, the cell will start firing because the only stable state is the relaxation limit cycle. After the kth oscillator starts firing, it becomes effectively coupled with its next neighbor $k + 1$, and, sequentially, all silent relaxation cells will oscillate and synchronize rapidly.

9. Conclusions

Coupled discrete electrochemical oscillators[16,27] and continuous electrochemical systems[14] are capable of synchronizing in different synchronization modes. As a result, a variety of spatio-temporal behavior can be observed, depending on the geometric and electric characteristics of the system. In the present work, it was shown that the rate of synchronization, the persistence of synchronization modes under small phase and period differences, and the response under external perturbations are crucially influenced by the relaxation character of the oscillators. As a result, specific spatio-temporal features are induced and manipulated by utilizing the unique synchronization properties of coupled relaxation oscillations. More specifically, it was shown that rings of discrete electrochemical oscillators are coupled only electrically if $\delta \ll w$ and $\beta = 2\pi w/l \ll 1$ (where δ is the length of the diffusion layer, w the distance between the working electrode and the reference electrode, and l the ring radius), the coupling is next-neighbor, symmetric, and linear, and the coupling strength is determined by the conductivity of the electrolytic solution and the geometric characteristics $(\sigma\beta/(3h))$.

Under these constraints, the results can be summarized as follows.

(1) Networks of identical relaxation oscillators synchronize rapidly in-phase by a compensation of initial phase differences.

(2) Networks of slightly nonidentical relaxation oscillators synchronize rapidly in-phase by a compensation of period differences.

(3) Networks of relaxation oscillators with groups under almost anti-phase initial conditions synchronize groupwise anti-phase. A spatial pattern imposed by the initial conditions is preserved.

(4) Specific spatial patterns can be imposed or imputed to a network of relaxation oscillators by perturbing the appropriate cell groups in anti-phase instances.

(5) Imposed spatial patterns can be removed from a network of relaxation oscillators or corrected by perturbing the appropriate cells in out-of-phase instances.

(6) Synchronized spiking is induced when silent relaxation cells are coupled with quiescent cells.

Appendix A

Transport Simplifications. Let us consider the boundary value problem defined by eqs 1−4. This problem can be simplified significantly by introducing several assumptions. Thus, the total current density flowing through the system is given by[28]

$$\boldsymbol{i}(x, y, z, t) = -F\sum_{m=1}^{M} n_m D_m \nabla c_m - F^2 \sum_{m=1}^{M} n_m^2 \gamma_m c_m \nabla\Phi \quad \text{(A.1)}$$

If all diffusion coefficients are assumed equal $(D_1 = ... = D_M = D)$,

$$\boldsymbol{i}(x, y, z, t) = -FD\nabla\sum_{m=1}^{M} n_m c_m - F^2 \sum_{m=1}^{M} n_m^2 \gamma_m c_m \nabla\Phi \quad \text{(A.2)}$$

Under the assumption of electroneutrality, $\sum_{m=1}^{M} n_m c_m \approx 0$, the following relation is obtained:

$$\boldsymbol{i}(x, y, z, t) = -F^2 \sum_{m=1}^{M} n_m^2 \gamma_m c_m \nabla\Phi \quad \text{(A.3)}$$

Note that the aforementioned approximation holds, because the summation in the first right-hand term of eq A.2 is a very small number that is multiplied by FD, which is on the order of unity. If we further assume that the conductivity $\kappa = F^2\sum_{m=1}^{M} n_m^2 \gamma_m c_m$ is approximately constant, even in regions of varying concentration, then

$$\boldsymbol{i}(x, y, z, t) = -\kappa\nabla\Phi \tag{A.4}$$

Because of the equation of conservation of charge, $\nabla\cdot\boldsymbol{i} = 0$, the following relation is obtained for the potential:

$$\nabla^2\Phi = 0 \tag{A.5}$$

The Laplace equation is valid only in regions where concentration gradients are completely absent and the conductivity is independent of space.[29] Nevertheless, it is expected that Eq. (A.5) holds approximately for the potential if the diffusion coefficients of the ionic species are almost equal and the conductivity κ is approximately constant, even in regions of varying c_m. Under the assumption of constant κ, eq 1 is written

$$\frac{\partial c_m}{\partial t} = D\nabla^2 c_m + \frac{t_m\kappa}{n_m F}\nabla^2\Phi \tag{A.6}$$

where t_m is the transport number of the mth species. Using eq A.5, eq A.6 transforms to the diffusion equation,

$$\frac{\partial c_m}{\partial t} = D\nabla^2 c_m \tag{A.7}$$

Equations A.5 and A.7 may be substituted into eq 1 and the boundary condition eq 2 may be replaced by

$$j_{F,m} + j_{C,m} = -D\left.\frac{\partial c_m}{\partial z}\right|_{z=0} - \frac{t_m\kappa}{n_m F}\left.\frac{\partial\Phi}{\partial z}\right|_{z=0} \tag{A.8}$$

Multiplying eq A.8 by Fn_m and summing over all species under the condition $\sum_{m=1}^{M} t_m = 1$, we obtain

$$i_F + i_C = -\kappa\left.\frac{\partial\Phi}{\partial z}\right|_{z=0} \tag{A.9}$$

where $i_C = C_{DL}(\partial\Delta\Phi_{DL}/\partial t)$, C_{DL} is the specific capacitance of the double layer, and $\Delta\Phi_{DL}$ is the potential drop at the double layer. We can observe that eqs A.5 and A.7 are coupled only through the surface concentration $c_m(x, y, z = 0, t)$ and its derivatives at that point. The problem is thus reduced to determining $c_m(x, y, z = 0, t)$ and its derivative at $z = 0$ and then solving eq A.5 for every t.

Simplification of the Diffusion Layer. We proceed by taking the spatial average of eq A.7 along the z-coordinate over a region extending from $z = 0$ to $z = \delta$:

$$\frac{\partial}{\partial t}\int_0^\delta c_m\,dz = D\int_0^\delta\left(\frac{\partial^2 c_m}{\partial x^2} + \frac{\partial^2 c_m}{\partial y^2}\right)dz + D\left.\frac{\partial c_m}{\partial z}\right|_{z=\delta} - D\left.\frac{\partial c_m}{\partial z}\right|_{z=0} \tag{A.10}$$

which, using eq A.8, is written

$$\frac{\partial}{\partial t}\int_0^\delta c_m\,dz = D\int_0^\delta\left(\frac{\partial^2 c_m}{\partial x^2} + \frac{\partial^2 c_m}{\partial y^2}\right)dz + D\left.\frac{\partial c_m}{\partial z}\right|_{z=\delta} + \frac{t_m\kappa}{n_m F}\left.\frac{\partial\Phi}{\partial z}\right|_{z=0} + j_{F,m} + j_{C,m} \tag{A.11}$$

We further assume that the region from $z = 0$ to $z = \delta$ coincides with the Nerst diffusion layer, where the concentration profile is approximately linear along the z-coordinate:

$$c_m(x, y, z, t) = c_m(x, y, z = 0, t) + \frac{c_{b,m} - c_m(x, y, z = 0, t)}{\delta}z \tag{A.12}$$

Using this approximation, we obtain

$$\left.\frac{\partial c_m}{\partial t}\right|_{z=0} = \frac{2D}{\delta^2}(c_{b,m} - c_m(x, z = 0, t)) + D\left.\frac{\partial^2 c_m}{\partial x^2}\right|_{z=0} + D\left.\frac{\partial^2 c_m}{\partial y^2}\right|_{z=0} + \frac{2t_m\kappa}{n_m F\delta}\left.\frac{\partial\Phi}{\partial z}\right|_{z=0} + \frac{2}{\delta}j_{F,m} + \frac{2}{\delta}j_{C,m} \tag{A.13}$$

Equation A.13 may replace eqs A.7 and A.8. The problem, thus, reduces to solving eq A.5 with the boundary conditions given in eqs 3, 4, A.9, and A.13.

Geometric Simplifications. We simplify the system even further by assuming that the working electrode is a ring with radius l. In addition, we consider the reference electrode to be an infinite plane located at a distance $z = w$. Because of symmetry, the y-coordinate can be ignored and all dynamic variables are dependent only on the spatial variables x and z. Furthermore, we assume $j_{C,k} = 0$ and that both i_F and $j_{F,m}$ are functions of the surface potential and only one reacting species, $c_1(x, z = 0, t)$.

In dimensionless form, the problem is rewritten as

$$\beta^2\frac{\partial^2\varphi}{\partial x^2} + \frac{\partial^2\varphi}{\partial z^2} = 0 \tag{A.14}$$

where, in eq A.14, x and z ($x \rightarrow (2\pi/l)x$ and $z \rightarrow z/w$) are the dimensionless spatial coordinates, $\varphi = (F/RT)\Phi$ is the dimensionless potential, and $\beta = 2\pi w/l$. Furthermore, let us consider potentiostatic conditions

$$\upsilon = u(x, t) + \varphi(x, z = 0, t) \tag{A.15}$$

where $\upsilon = (F/RT)V$ is the dimensionless applied potential on the ring electrode and $u = (F/RT)\Delta\Phi_{DL}$ is the dimensionless potential drop in the double layer. The boundary conditions are written as

$$\varphi(x, z = 1) = 0 \tag{A.16a}$$

$$\varphi(x, z) = \varphi(x + 2\pi, z) \tag{A.16b}$$

together with the equation of conservation of charge, eq A.9,

$$\epsilon\frac{\partial u}{\partial t} = -\frac{\sigma}{\beta}\left.\frac{\partial\varphi}{\partial z}\right|_{z=0} - i_F(u, c) \tag{A.17}$$

and the mass balance, eq A.13,

$$\left.\frac{\partial c}{\partial t}\right|_{z=0} = 1 - c(x, z = 0, t) - \frac{t_c\sigma}{\beta}\left.\frac{\partial\varphi}{\partial z}\right|_{z=0} + j_F(u, c) + \frac{\beta^2\xi^2}{2}\left.\frac{\partial^2 c}{\partial x^2}\right|_{z=0} \tag{A.18}$$

In eq A.17, $\sigma = [2\pi\delta RT/(F^2Dc_{b,1}l)]\kappa$, $\epsilon = 2C_{DL}RT/(F^2c_{b,1}\delta)$, and $n_1 = 1$. The dimensionless function $i_F \rightarrow [\delta/(FDc_{b,1})]i_F$ represents the total faradaic current and it is implicitly a function of x and t, through its dependence on the double-layer potential, $u(x, t)$, and surface concentration, $c(x, z = 0, t) = (c_1(x, z=0, t)/c_{b,1})$. Similarly, $j_F \rightarrow [\delta/(Dc_{b,1})]j_F$ is the dimensionless flux that is due to the faradaic reaction of the reacting species. The parameter $t \rightarrow (2D/\delta^2)t$ represents the dimensionless time and $\xi = \delta/w$.

The aforementioned boundary value problem (eqs A.14−A.18) is spatially two-dimensional. The solution of eq A.14, together with the boundary conditions given in eqs A.16, can be obtained by the method of separation of variables. Hence,

$$\varphi(x, z, t) = A_0(t)(1 - z) + \sum_{n=1}^{\infty}[A_n(t) \sin nx + B_n(t) \cos nx]\sinh n\beta(z - 1) \quad \text{(A.19)}$$

where the dependence on time is introduced through the Fourier coefficients. Using eq A.19, it can be shown[18−20] that, under the condition of $0 < |n\beta| < \pi$, eqs A.17 and A.18 are written as

$$\epsilon\frac{\partial u(x, t)}{\partial t} = \frac{\sigma}{\beta}[v - u(x, t)] + \frac{\sigma\beta}{3}\frac{\partial^2 u(x, t)}{\partial x^2} - i_F(u, c) \quad \text{(A.20)}$$

$$\left.\frac{\partial c(x, z, t)}{\partial t}\right|_{z=0} = 1 - c(x, z = 0, t) + \left.\frac{\beta^2\xi^2}{2}\frac{\partial^2 c(x, z, t)}{\partial x^2}\right|_{z=0} - \frac{t_c\sigma}{\beta}[v - u(x, t)] - \frac{t_c\sigma\beta}{3}\frac{\partial^2 u(x, t)}{\partial x^2} + j_F(u, c) \quad \text{(A.21)}$$

where the spatial coordinate z is not longer a variable of the system. Thus, under the aforementioned assumptions, the problem is reduced to the solution of eqs A.20 and A.21, which is spatially one-dimensional.

Transformation to a Discrete Network. Setting $h = \Delta x^2$, where $\Delta x = 2\pi/N$, eq A.20 can be written in a discrete form, using a three-point symmetric discretization scheme:

$$\epsilon\frac{du^{(k)}}{dt} = \frac{\sigma}{\beta}(v - u^{(k)}) - i_F(u^{(k)}, c^{(k)}) + \frac{\sigma\beta}{3h}(u^{(k-1)} - 2u^{(k)} + u^{(k+1)}) \quad \text{(A.22)}$$

for $k = 1, 2, ..., N$ and $u^{(1)} = u^{(N+1)}$, $c^{(1)} = c^{(N+1)}$ due to the ring geometry. Equation A.22 represents a system of *discrete* cells that are communicating via next-neighbor coupling. The coupling strength is given by $\sigma\beta/(3h)$ and, thus, is dependent on the conductivity of the medium, the aspect ratio of the cell, and the distance between the neighbors. Equation A.22 can be written also as

$$\epsilon\frac{du^{(k)}}{dt} = \frac{\sigma}{\beta}(v - u^{(k)}) - i_F(u^{(k)}, c^{(k)}) + \frac{\sigma\beta}{3h}\sum_{\substack{m=k-1 \\ m\neq k}}^{k+1}(u^{(m)} - u^{(k)}) \quad \text{(A.23)}$$

As can be seen, under the condition of small β, the effect of coupling is localized and, upon discretization, becomes next-neighbor, symmetric, and linear. For fixed h, σ, and l, coupling is enhanced as β becomes bigger (that is, as the reference electrode is brought away from the surface (increasing w) of the ring). In the absence of coupling, eq A.23 corresponds to the usual ODE that describes only temporal variations of the double-layer potential, where the first right-hand term corresponds to the total current flowing through the cell and the second corresponds to the total faradaic current. The case of variable distance between the cells is treated in Appendix B.

Similarly, eq A.21 is written as

$$\frac{dc^{(k)}}{dt} = 1 - c^{(k)} - \frac{t_c\sigma}{\beta}(v - u^{(k)}) + j_F(u^{(k)}, c^{(k)}) + \frac{\beta^2\xi^2}{2h}\sum_{\substack{m=k-1 \\ m\neq k}}^{k+1}(c^{(m)} - c^{(k)}) - \frac{t_c\sigma\beta}{3h}\sum_{\substack{m=k-1 \\ m\neq k}}^{k+1}(u^{(m)} - u^{(k)}) \quad \text{(A.24)}$$

Appendix B

If we allow a nonuniform grid along the x-coordinate, the coupling strength can become a function of the position along this grid.

Let us expand $u^{(k+1)}$ in a Taylor series around $u^{(k)}$:

$$u^{(k+1)} = u^{(k)} + \frac{\partial u^{(k)}}{\partial x}(x^{(k+1)} - x^{(k)}) + \frac{1}{2}\frac{\partial^2 u^{(k)}}{\partial x^2}(x^{(k+1)} - x^{(k)})^2 + ... \quad \text{(B.1)}$$

A similar expansion of $u^{(k-1)}$ around $u^{(k)}$ gives

$$u^{(k-1)} = u^{(k)} + \frac{\partial u^{(k)}}{\partial x}(x^{(k-1)} - x^{(k)}) + \frac{1}{2}\frac{\partial^2 u^{(k)}}{\partial x^2}(x^{(k-1)} - x^{(k)})^2 + ... \quad \text{(B.2)}$$

Setting $x^{(k+1)} - x^{(k)} = r_{k+1}\Delta x$ and $x^{(k)} - x^{(k-1)} = r_{k-1}\Delta x$, eqs B.1 and B.2 become

$$u^{(k+1)} = u^{(k)} + \frac{\partial u^{(k)}}{\partial x}r_{k+1}\Delta x + \frac{1}{2}\frac{\partial^2 u^{(k)}}{\partial x^2}r_{k+1}^2\Delta x^2 + ... \quad \text{(B.3)}$$

and

$$u^{(k-1)} = u^{(k)} - \frac{\partial u^{(k)}}{\partial x}r_{k-1}\Delta x + \frac{1}{2}\frac{\partial^2 u^{(k)}}{\partial x^2}r_{k-1}^2\Delta x^2 + ... \quad \text{(B.4)}$$

Starting from the general equation[30]

$$\frac{\partial^2 u^{(k)}}{\partial x^2} = Pu^{(k-1)} + Qu^{(k)} + Ru^{(k+1)} \quad \text{(B.5)}$$

and using eqs B.3 and B.4, we obtain

$$\frac{\partial^2 u^{(k)}}{\partial x^2} = (P + Q + G)u^{(k)} + (Pr_{k-1} + Gr_{k+1})\Delta x\frac{\partial u^{(k)}}{\partial x} + (Pr_{k-1}^2 + Gr_{k+1}^2)\frac{\Delta x^2}{2}\frac{\partial^2 u^{(k)}}{\partial x^2} \quad \text{(B.6)}$$

The most accurate approximation is obtained by setting

$$P + Q + G = 0$$
$$-Pr_{k-1} + Gr_{k+1} = 0$$
$$(Pr_{k-1}^2 + Gr_{k+1}^2)\frac{\Delta x^2}{2} = 1$$

Determining the coefficients P, Q, and G and inserting them back into eq B.6, we obtain, for the coupling term,

$$\frac{\partial^2 u^{(k)}}{\partial x^2} = \frac{2u^{(k-1)}}{r_{k-1}(r_{k+1} + r_{k-1})\Delta x^2} - \frac{2u^{(k)}}{r_{k+1}r_{k-1}\Delta x^2} + \frac{2u^{(k+1)}}{r_{k+1}(r_{k+1} + r_{k-1})\Delta x^2} \quad \text{(B.7)}$$

For $r_{k-1} = r_{k+1} = 1$, eq B.7 changes into the form of eq A.23.

Acknowledgment. The work was sponsored by the Greek Secretariat of Research and Technology and the Op. P. "Com"

and by the Research for the Future (RFTF) Program of the Japan Society for the Promotion of Science. The constant support and encouragement of Prof. Y. Chryssoulakis to A.K. and the useful comments of Dr. D. Komilis on the manuscript are especially acknowledged.

References and Notes

(1) Kopell, N.; Somers, D. *J. Math. Biol.* **1995**, *33*, 261.
(2) Somers, D.; Kopell, N. *Biol. Cybern.* **1993**, *68*, 393.
(3) Somers, D.; Kopell, N. *Physica D* **1995**, *89*, 169.
(4) Hoppensteadt, F. C.; Izhikevich, E. M. *Weakly Connected Neural Networks*; Applied Mathematical Sciences, Vol. 126; Springer−Verlag: New York, 1997.
(5) Izhikevich, E. M. *Int. J. Bifurcation Chaos Appl. Sci. Eng.* **2000**, *10*, 2553.
(6) Abbott, L. F. *J. Phys. A* **1990**, *23*, 3835.
(7) Grasman, J.; Jansen, M. J. W. *J. Math. Biol.* **1979**, *7*, 171.
(8) Ostwald, W. *Z. Phys. Chem.* **1900**, *35*, 333.
(9) Lillie, R. S. *J. Gen. Physiol.* **1920**, *3*, 107.
(10) Lillie, R. S. *J. Gen. Physiol.* **1925**, *7*, 473.
(11) Franck, U. F. *Prog. Biophys. Chem.* **1956**, *6*, 171.
(12) Okamoto, H.; Tanaka, N.; Naito, M. *Chem. Phys. Lett.* **1995**, *237*, 432.
(13) Amatore, C.; Brown, A. R.; Thouin, L.; Warkocz, J.-S. *C. R. Acad. Sci., Ser. IIc: Chim.* **1998**, *1*, 509.
(14) Christoph, J.; Eiswirth, M. *Chaos* **2002**, *12*, 215.
(15) Krischer, K. In *Advances in Electrochemical Science and Engineering*; Alkire, R. C., Kolb, D. M., Eds.; Wiley-VCH Verlag, 2002; Vol. 8, pp 89−208.
(16) Karantonis, A.; Miyakita, Y.; Nakabayashi, S. *Phys. Rev. E* **2002**, *65*, 046213.
(17) Miyakita, Y.; Karantonis, A.; Nakabayashi, S. *Chem. Phys. Lett.* **2002**, *362*, 461.
(18) Karantonis, A.; Bieniasz, L.; Nakabayashi, S. *Phys. Chem. Chem. Phys.* **2003**, *5*, 1831.
(19) Mazouz, N.; Flätgen, G.; Krischer, K. *Phys. Rev. E* **1997**, *55*, 2260.
(20) Orlychenko, O.; Ye, Y.; Chang, H.-C. *Phys. Rev. E* **1998**, *57*, 5196.
(21) Doedel, E. J.; Champneys, A. R.; Fairgrieve, T. F.; Kuznetsov, Y. A.; Sandstede, B.; Wang, X. *AUTO 97: Continuation and Bifurcation Software for Ordinary Differential Equations*, Technical Report, Concordia University, Montreal, Quebec, Canada, 1997.
(22) Ermentrout, G. B.; Kopell, N. *J. Math. Biol.* **1991**, *29*, 195.
(23) Izhikevich, E. M. *SIAM J. Appl. Math.* **2000**, *60*, 1789.
(24) Kuramoto, Y. *Chemical Oscillators, Waves, and Turbulence*; Springer−Verlag: Berlin, 1984.
(25) Williams, T. L.; Bowtell, G. *J. Comput. Neurosci.* **1997**, *4*, 47.
(26) Press: W. H.; Teukolsky, S. A.; Vetterling, W. T.; Flannery, B. P. *Numerical Recipes in Fortran 77. The Art of Scientific Computing*, 2nd ed.; Cambridge University Press: Cambridge, U.K., 1997.
(27) Kiss, I. Z.; Wang, W.; Hudson, J. L. *J. Phys. Chem. B* **1999**, *103*, 11433.
(28) Levich, V. G. *Physicochemical Hydrodynamics*; Prentice−Hall: Englewood Cliffs, NJ, 1962.
(29) Newman, J. S. *Electrochemical Systems*, 2nd ed.; Prentice−Hall: Englewood Cliffs, NJ, 1991.
(30) Fletcher, C. A. J. *Computational Techniques for Fluid Dynamics*, 2nd ed.; Springer−Verlag: Berlin, 1991; Vol. 1.